GLOBAL BIOGEOCHEMICAL CYCLES, VOL. 23, GB4017, doi:10.1029/2008GB003405, 2009

Click Here for Full Article

Modeling the coupling of ocean ecology and biogeochemistry

S. Dutkiewicz,[1] M. J. Follows,[1] and J. G. Bragg[2,3]

Received 15 October 2008; revised 19 April 2009; accepted 14 July 2009; published 3 November 2009.

[1] We examine the interplay between ecology and biogeochemical cycles in the context of a global three-dimensional ocean model where self-assembling phytoplankton communities emerge from a wide set of potentially viable cell types. We consider the complex model solutions in the light of resource competition theory. The emergent community structures and ecological regimes vary across different physical environments in the model ocean: Strongly seasonal, high-nutrient regions are dominated by fast growing bloom specialists, while stable, low-seasonality regions are dominated by organisms that can grow at low nutrient concentrations and are suited to oligotrophic conditions. In the latter regions, the framework of resource competition theory provides a useful qualitative and quantitative diagnostic tool with which to interpret the outcome of competition between model organisms, their regulation of the resource environment, and the sensitivity of the system to changes in key physiological characteristics of the cells.

Citation: Dutkiewicz, S., M. J. Follows, and J. G. Bragg (2009), Modeling the coupling of ocean ecology and biogeochemistry, *Global Biogeochem. Cycles*, *23*, GB4017, doi:10.1029/2008GB003405.

1. Introduction

[2] Phytoplankton community structure in the world's ocean is understood to regulate important biogeochemical pathways, notably the export of organic carbon to the deep ocean. The contrast between blooms of aggregating and sinking diatoms and a population of picoplankton locked in a tightly coupled microbial loop is clearly important [e.g., *Pomeroy*, 1974; *Laws et al.*, 2000]. The quality of exported particles, for example their association with particular mineral ballast, is significant in setting the depth at which they are processed and respired [e.g., *Armstrong et al.*, 2002; *Klaas and Archer*, 2002]. Community structure, in turn, is strongly influenced by the physical and chemical environment; the availability of a variety of essential resources and the variability of the environment [*Margalef*, 1968; *Tozzi et al.*, 2004]. The ecology and biogeochemistry of the oceans are tightly interconnected. How is this complex, ecobiogeochemical system organized? How does the physical and chemical environment dictate ecological regimes? Numerical models of ocean biogeochemical cycles are a tool with which we can simulate aspects of this coupled system, elucidating and illustrating governing mechanisms and interactions [e.g., *Moore et al.*, 2002; *Le Quéré et al.*, 2005; *Hood et al.*, 2006]. Such numerical simulations can become sufficiently complex that we may need to return to more idealized frameworks to interpret them.

[3] Resource competition theory [*Tilman*, 1977] (pertinent aspects of which are briefly outlined in section 1.1) is an established ecological framework for considering the connections between ecology and resource availability. Recent empirical and theoretical studies [*Falkowski and Oliver*, 2007; *Litchman et al.*, 2007; *Irwin et al.*, 2006; *Wilson et al.*, 2007, and references therein; *Tozzi et al.*, 2004] emphasize the application of resource competition theory as a framework for interpreting the regulation of phytoplankton community structure.

[4] Here we examine a model of marine ecosystems (described further in section 1.2) in which phytoplankton community structure is explicitly "self-assembling" [*Follows et al.*, 2007]. A relatively large number of phytoplankton types are initialized each with physiological traits and functionalities stochastically chosen from plausible ranges. A subset of the virtual organisms persist at high abundances, according to their ability to compete for resources and susceptibility to predation, among many other factors. We ask to what extent is resource competition theory a qualitative and quantitative tool with which to interpret this complex and flexible ecosystem model?

1.1. Resource Competition Theory

[5] Resource competition theory [*Tilman*, 1977, 1982] provides a framework for interpreting the relationship between organisms and their resource environment. Here we recap some essential elements using a highly simplified example that implicitly assumes a local balance where the physical transport of organisms can be neglected. Consider

[1]Department of Earth, Atmospheric and Planetary Sciences, Massachusetts Institute of Technology, Cambridge, Massachusetts, USA.
[2]Department of Civil and Environmental Engineering, Massachusetts Institute of Technology, Cambridge, Massachusetts, USA.
[3]Now at CSIRO Plant Industry, Canberra, ACT, Australia.

Copyright 2009 by the American Geophysical Union.
0886-6236/09/2008GB003405$12.00

a single photoautotroph (P), nourished by a single macronutrient (N) which is supplied to the system with the rate S:

$$\frac{dN}{dt} = -\mu_m \frac{N}{N+\kappa_N} P + S \tag{1}$$

$$\frac{dP}{dt} = \mu_m \frac{N}{N+\kappa_N} P - mP \tag{2}$$

Here, μ_m is a maximal growth rate, a function of light and temperature. Nutrient limitation is parameterized as a Monod function where κ_N is the half-saturation constant, and m represents a simple parameterization of sinking, grazing, viral lysis and other loss terms (While we illustrate the theory assuming simple Monod growth, we note that analogous expressions can also be obtained when assuming a flexible internal stores model [see *Tilman*, 1977]). In completely steady conditions, when the system has come to equilibrium,

$$\overline{N} = \frac{\kappa_N m}{\mu_m - m} = R^* \tag{3}$$

$$\overline{P} = \frac{S}{m} \tag{4}$$

The equilibrium resource concentration, $\overline{N}$, is often denoted by R^* [*Tilman*, 1977]. Equation (3) suggests that the ambient concentration of the limiting resource is determined by characteristics of the organism including its maximum growth rate (μ_m), nutrient half-saturation constant (κ_N), and mortality rate (m). The equilibrium assumes a tight coupling of source and sink terms, so R^* reflects a combination of both bottom-up (κ_N, μ_m) and top-down (m) characteristics. If multiple organism types are present the ambient resource concentration will be drawn down to the lowest R^* amongst the organisms present and other organisms will be excluded over time [*Stewart and Levin*, 1973]. In the presence of multiple, potentially limiting resources coexistence can occur [*Tilman*, 1977] up to the number of resources (or other limiting factors [*Armstrong and McGehee*, 1980]). The organisms that dominate in this steady state limit, where competitive outcomes are determined by the ability to compete for limited resources, will be referred to here as "K strategy" types [*McArthur and Wilson*, 1967; *Kilham and Hecky*, 1988]. (See *McArthur and Wilson* [1967] for a description of "r" versus "K" selection and *Kilham and Hecky* [1988] for discussion of its application in phytoplankton ecology, and relation to R^* theory.)

[6] Should we expect that, in the marine environment, phytoplankton with the lowest R^* will dominate in a given environment? The ocean is never at rest, continually perturbed over vast range of timescales, from microscopic turbulence through to global change on geological timescales. What determines the outcome of competition in a variable environment?

[7] Contrast the steady state limit with a highly seasonal environment. At the initiation of a spring bloom, dissolved nutrients may not be limiting, $\frac{N}{N+\kappa_N} \sim 1$, and the grazer population small, $m \ll \mu_m$. In these conditions, equation (2) reduces to suggest that the fitness of a particular phytoplankton type, P, is related to its per capita growth rate, depends only on μ_m:

$$\frac{1}{P}\frac{dP}{dt} \sim \mu_m. \tag{5}$$

In this limit, organisms most able to take advantage of the abundant nutrients will dominate [*Stewart and Levin*, 1973]. We will refer to these organisms as "r strategy" types [*McArthur and Wilson*, 1967; *Kilham and Hecky*, 1988]. In high-nutrient regions, the organism with the fastest maximum growth rate, μ_m, will dominate in bloom periods [*Stewart and Levin*, 1973].

[8] Thus it seems likely that the utility of R^* in predicting competitive outcomes among marine phytoplankton and ambient nutrient concentrations will be restricted to certain ocean physical environments. Here we ask, using a complex, self-assembling model of the marine ecosystem and biogeochemical cycles, where and when is this framework of resource competition theory a useful tool? In what regions does it have qualitative and quantitative diagnostic power and what other factors determine the extent of those regions? To what extent does phytoplankton physiology regulate the nutrient environment of the oceans?

1.2. A Self-Assembling Model of Phytoplankton Communities

[9] We briefly describe the three-dimensional ocean model and some basic features of its biogeography. The model has been discussed previously by *Follows et al.* [2007]. It is based on a coarse resolution ($1° \times 1°$ horizontally, 24 levels) configuration of the MITgcm [*Marshall et al.*, 1997] constrained to be consistent with altimetric and hydrographic observations (the ECCO-GODAE state estimates [*Wunsch and Heimbach*, 2007]). We transport inorganic and organic forms of nitrogen, phosphorus, iron and silica, and resolve many tens of phytoplankton types as well as two simple grazers. The biogeochemical and biological tracers interact through the formation, transformation and remineralization of organic matter. Excretion and mortality transfer living organic material into sinking particulate and dissolved organic detritus which are respired back to inorganic form. The time-dependent change in the biomass of each of the many model phytoplankton types, P_j, is described in terms of a light-dependent, temperature-dependent, and resource-dependent growth, sinking, grazing, other mortality and transport by the fluid flow. (See Appendix A and *Follows et al.* [2007]).

[10] Many tens (here 78) of phytoplankton types are initialized with broad range of physiological attributes. The phytoplankton are assigned to one of two broad classes by random draw at the initialization of the model. A set of trade-offs are implemented (see Appendix A) that reflect empirical observations, and prevent the emergence of a single model organism that can dominate all habitats (the "Darwinian Demon"). We stochastically assign nutrient half-saturation constants (κ_N), light and temperature sensitivities from ranges of plausible values for these classes (Figure 1). Interactions with the environment, competition

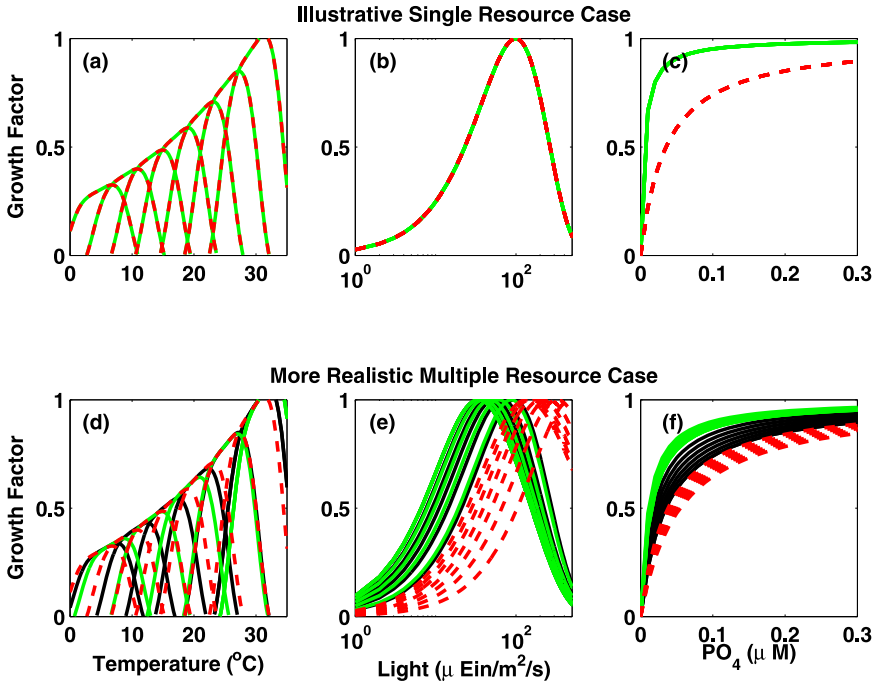

Figure 1. Growth of phytoplankton types $\mu = \mu_{\max}\gamma_T\gamma_I\gamma_N$ is controlled by temperature (γ_T), light (γ_I), and nutrients (γ_N). (a–c) "Single resource case." (d–f) "Multiple resource case." Green and black indicate K strategy phytoplankton types with low half-saturation constants and low maximum growth rate ($\mu_{\max}$). Red indicates r strategy phytoplankton types with high maximum growth rates and high half-saturation constants. In the single resource case, pairs of r and K strategy types are initialized with the same temperature sensitivity function and all have the same light sensitivity. In the multiple resource case, all parameters are randomly assigned from reasonable ranges, and green indicates small phytoplankton that cannot use nitrate (*Prochlorococcus* analogs) while black indicates those that can.

with other phytoplankton, and grazing determine the composition of the phytoplankton communities that persist in the model solutions.

[11] The system that emerges has plausible patterns of surface nutrients, biomass, primary and export production [*Follows et al.*, 2007; V. Saba et al., The challenges of modeling marine primary productivity through multidecadal climate shifts: A case study at BATS and HOT, submitted to *Global Biogeochemical Cycles*, 2009]. For instance, *Follows et al.* [2007] showed that the model analogs of *Prochlorococcus* (tiny picocyanobacteria of which many cannot utilize nitrate as a nitrogen source) occupied similar environmental habitats to real world ecotypes with appropriate ranking in relative abundance between ecotypes and, most importantly, with physiological attributes (light, temperature and nutrient growth sensitivities) specialized in the same way as their real world counterparts. This qualitative agreement suggests that the virtual ocean ecosystem is regulated in some significant respect by processes similar to those that structure real world ocean ecosystems.

[12] The model therefore seems sufficiently complex to reflect relevant properties of marine phytoplankton communities and natural interactions. On the other hand, it can be completely characterized and manipulated for transparent interpretation. It can serve as an ecological "laboratory" in which to explore the relevance of theoretical concepts of community structure and ecosystem-nutrient cycle interactions. Thus we will seek to interpret the regulation of community structure and environmental nutrient concentrations in the model using resource competition theory.

[13] To do so we first examine an illustrative configuration (see Table 1) of the model, in which we simplify the ocean biogeochemistry model to represent only a single macronutrient resource (analogous to nitrate or phosphate) and just two broad functional groups of phytoplankton (section 2). There we examine the applicability of resource competition theory as an organizing framework. Later (section 3), we reexamine the more realistic, multiple nutrient simulations of *Follows et al.* [2007] described here in the light of the illustrative study, focusing on the role of ecology and ecosystem dynamics in regulating the distributions of key nutrients.

2. Illustrative Case: Single Resource

[14] For illustrative purposes we first employ a simplified configuration of the global ecosystem and biogeochemistry model where growth is dependent on only one macronutrient resource which we call the "single resource" case. We retain the "self-assembling" ecosystem approach and initialize many phytoplankton types but reduce the breadth of physiological variety to encompass just two broad functional types.

[15] Here the prognostic equations follow those of the full system (Appendix A) but consider only a single resource, N_1, nominally phosphorus (results would be almost identical

Table 1. List of Model Experiments[a]

	Brief Description	Types of Phytoplankton[b]	Sensitivity Studies
Illustrative single resource case	PO_4 only, phytoplankton given nonrandom growth parameters	1. K strategy (low R^*) 2. r strategy (fast growing)	double κ_{N_1} halve κ_{N_1}
Multiple resource case	PO_4, NO_3, NO_2, NH_4, Fe, Si random assignment of phytoplankton growth parameters	1. small, low R^* 2. small, no NO_3, lowest R^* (" *Prochlorococcus* analogs") 3. large, fast growing 4. large, fast growing, use silica ("diatoms analogs")	double all κ_{N_i} halve all κ_{N_i}

[a]The columns indicate the biogeochemical and ecological scope of the configuration studied; the degree of richness in the functionality of the initialized phytoplankton populations; and the sensitivity studies performed using each basic configuration, respectively. Parameter descriptions and values are given in Tables 2 and 3.
[b]Numbers indicate that phytoplankton types are grouped together as functional types.

if we used nitrate as our only nutrient instead), and a single grazer, Z_1. The model is initialized with 78 phytoplankton types in two functional groups (Table 1): Half are initialized as "r strategy" types with high maximum growth rate and phosphate half-saturation ($\mu_{\max} = 2.5\ d^{-1}$; $\kappa_{N_1} = 3.5 \times 10^{-3}\ \mu M\ P$; see Table 2). The other half initialized as "K strategy" types with low maximum growth rate and phosphate half-saturation ($\mu_{\max} = 1.4\ d^{-1}$; $\kappa_{N_1} = 0.5 \times 10^{-3}\ \mu M\ P$). We note that with these choices, the nutrient affinity ($\mu_{\max}/\kappa_{N_1}$) is almost 4 times greater for the "K strategy" types than the r strategist in oligotrophic conditions.

[16] In this configuration all initialized phytoplankton are given the same light sensitivity of growth and the same susceptibility to predation by a single grazer. The temperature sensitivities of growth for the phytoplankton types (Figure 1a) are initialized so that some are optimal in all regions and seasons of the model ocean, and are specified so that an r and a K strategist type have the same optima and range. Thus there are 39 initialized "pairs" of phytoplankton types. Each pair is physiologically identical except for the phosphorus half-saturation (κ_{N_1}) and maximum growth rate ($\mu_{\max}$). Each pair effectively represents an "r strategy" and a "K strategy" complement.

[17] All of the phytoplankton types are initialized with identical, low biomass distributions and the phosphate field is initialized from climatology [*Conkright et al.*, 2002]. The model is integrated forward for 10 years. After about 2 years the phytoplankton types begin to occupy clearly different biogeographical regions, and after several years exhibit a repeating seasonal cycle. Here we discuss results from the tenth year of integration. Longer integrations of the model reveal that the biogeography of the model changes very

Table 2. Ecosystem Model Parameters That Vary Between Experiments and/or Phytoplankton Types[a]

Parameter	Symbol	Single Resource Case	Multiple Resource Case	Units
Maximum Phyto growth rate	$\mu_{\max}$	K: 1.4 r: 2.5	S: 1.4 L: 2.5	d^{-1} d^{-1}
PO_4 half-saturation coefficient	κ_{PO4}	K: 0.5 * 10^{-3} r: 3.5 * 10^{-3}	S: range 0.015 to 0.035 L: range 0.035 to 0.055 C: range 0.01 to 0.015	μ M P μ M P μ M P
Temperature optimum coefficient	T_o	K: evenly −2 to 30 r: evenly −2 to 30	S: range −2 to 30 L: range −2 to 30	°C °C
PAR saturation coefficient	k_{par}	K: 0.012r: 0.012	S: mean 0.012, std 0.02 L: mean 0.012, std 0.006	(μEin m^{-2} s^{-1})$^{-1}$ (μEin m^{-2} s^{-1})$^{-1}$
PAR inhibition coefficient	k_{inhib}	K: 1 * 10^{-3} r: 1 * 10^{-3}	S: mean 6 * 10^{-3}, std 1 * 10^{-4} L: mean 1 * 10^{-3}, std 5 * 10^{-5}	
Phytoplankton elemental ratios	$R_{Si:P}$ $R_{N:P}$ $R_{Fe:P}$	---	D: 16 16 1.25 * 10^{-3}	
Half-saturation coefficients	κ_{NO3} κ_{NH4} κ_{Fe} κ_{Si}	----	$R_{N:P}$ * κ_{PO4} $\frac{1}{2}R_{N:P}$ * κ_{PO4} $R_{Fe:P}$ * κ_{PO4} D: $R_{Si:P}$ * κ_{PO4}	μM N μM N μM Fe μM Si
Phyto Sinking rate	w^P	K: 0 r: 0	S: 0 L: 0.5	m d^{-1} m d^{-1}
Phytoplankton palatability	η	K: 1 r: 1	S: 1 L: 0.9 D: 0.8	
DOM/POM partitioning	λ_{mp} λ_{mz} λ_g	K: 0.2 r: 0.5	S: 0.2 L: 0.5	
Temperature range coefficient	B	K: 3 * 10^{-4} r: 3 * 10^{-4}	S: 1 * 10^{-3} L: 3 * 10^{-3}	°C^{-1} °C^{-1}

[a]For single resource case, "K" indicates K strategy types, "r" indicates r strategy types. For multiple resource case, S, L, D, C indicate "small," "large," "diatom analogs," and " *Prochlorococcus* analogs," respectively. Note that unless stated, C has same values as S, and D has same values as L. "Range" indicates that values are chosen randomly from within this range.

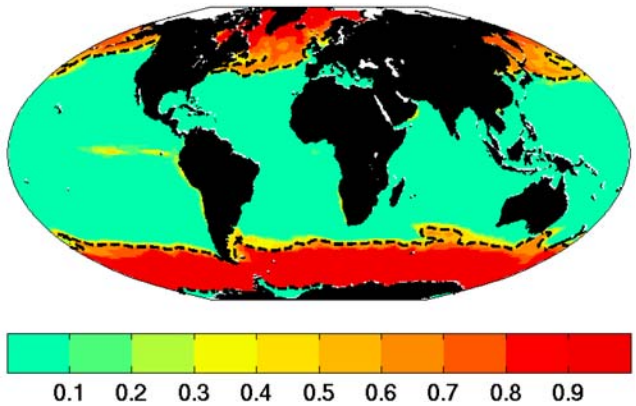

Figure 2. Single resource case: Fraction of biomass in r strategy types relative to total. The dashed contour indicates 0.5, separating regions where r and K strategies dominate.

little between a decade and two hundred years, thus we consider this to be a quasi-stable state. The annual surface phosphate distribution is plausible, with elevated concentrations in upwelling regions, while subtropics and tropics are oligotrophic. Some details, for example the High-Nitrate Low-Chlorophyll (HNLC) regions, are affected by the lack of additional micronutrient controls.

2.1. Single Resource Case: Biogeography

[18] Fast growing (r strategy) phytoplankton types dominate the annual biomass in the strongly seasonal, high-latitude regimes while the low half-saturation (K strategy) types dominate the more oligotrophic, low latitudes (Figure 2). The division between the two ecological regimes (the 0.5 contour in Figure 2) is closely associated with the maximum gradient in the annually averaged surface macronutrient concentration, reflecting the contrasting nutrient affinity and growth rates of the two imposed functional groups. The sharp transition between ecological regimes reflects the idealization with just two functional groups. In the Southern Hemisphere, the region where the r strategy types completely dominate coincides with the physical region of positive upwelling in the Southern Ocean.

2.2. Single Resource Case: R^* Analysis

[19] We expect the steady state analysis of resource competition theory to be most applicable (if at all) in the low-seasonality, oligotrophic regions where K strategy types dominate. Assuming steady state in equation (A2) and neglecting transport terms, we develop a diagnostic R_j^* (see Appendix A (section A6) for derivation) which may be evaluated for each of the 78 initialized phytoplankton types (j = 1, 2,...78) in the global model. This diagnostic is analogous to R^* (equation (3)) but accounts for the relatively complex loss terms (see equation (A2), though note that there is only one nutrient and one grazer in this illustrative case) which include explicit terms in P_j and Z_1 which can only be determined diagnostically in the numerical model.

$$R_j^* = \frac{\kappa_{N_{1_j}} L_j}{\nu_j - L_j}, \tag{6}$$

where for this single nutrient, single grazer case

$$\nu_j = \mu_{\max_j} \gamma_j^T \gamma_j^I \tag{7}$$

$$L_j = m_j^p + \frac{1}{P_j}\frac{\partial w_j^p P_j}{\partial z} + g_{\max_j}\frac{\eta_j}{A_1}\frac{A_1}{A_1 + \kappa_1^P} Z_1. \tag{8}$$

Here the growth term, ν_j, is a function of temperature and light and the loss term, L_j, includes mortality, sinking and grazing. This loss term is a function of the abundance of the jth phytoplankton, the total palatability weighted abundance of phytoplankton, A_1, and the abundance of the grazer Z_1. In essence R^* is still a combination of the phytoplankton physiology and the loss terms, however the nonlinearity means that R^* is no longer independent of the phytoplankton and source terms.

[20] Resource competition theory, as discussed in the Introduction, suggests the following: (1) Organisms with the lowest R^* will outcompete all others for a single limiting resource, and without other limiting factors will exclude them, (2) the ambient concentration of that resource will be set to the minimum R^*, and (3) and the resource will vary predictably with changes in the physiology of the lowest-R^*

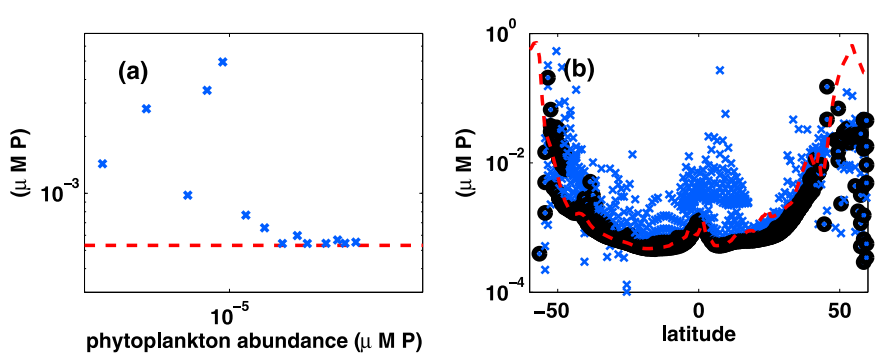

Figure 3. Single resource case R^* Analysis: (a) Single location (circle in Figure 5): R_j^* for each phytoplankton (crosses), averaged for February (0–50 m). Red dashed line indicates the February (0–50 m) averaged nutrient concentration at that location. (b) Pacific transect (line in Figure 5): R_j^* for each phytoplankton (blue crosses), averaged 0–50 m for February for each latitude; phytoplankton with biomass at least 10% of the maximum at that location are indicated additionally with a black circle; red dashed line indicates February (0–50 m) nutrient concentration.

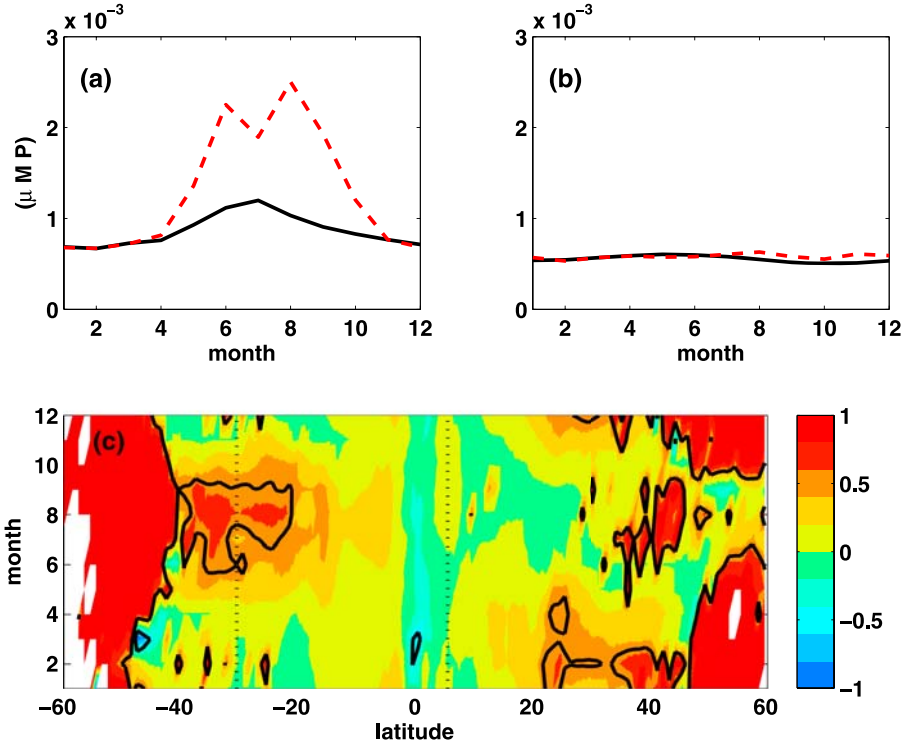

Figure 4. Single resource case: (a) Time series of nutrient concentration (red dashed) and minimum diagnosed R^*_j ($R^*_{\min}$, black solid) for 0–50 m at 211°W, 31°S (marked on Figure 5). (b) Same as above but for 211°W, 5°N. (c) Pacific transect (marked on Figure 5): Relative difference between diagnosed $R^*_{\min}$ and ambient nutrient, both averaged for 0–50 m for each month, $(N_1 - R^*_{\min})/N_1$. Contours are at (−0.5, 0.5), green/yellow shading indicates $R^*_{\min}$ close to ambient nutrient, red indicates nutrients exceed $R^*_{\min}$, and blue indicates that nutrients are less than the $R^*_{\min}$; no shading indicates where no reasonable value for the diagnosed $R^*_{\min}$ was found. Dotted lines indicate locations for Figures 4a and 4b.

organisms. We examine the global model in the context of these hypotheses. In the following paragraphs we examine how resource competition theory helps us to interpret the model ecosystem first locally for a single grid point, then with latitude and season. Afterward we interpret the large-scale regional patterns.

[21] We first consider the characteristics of phytoplankton types at a single grid cell in the Equatorial Pacific in the month of February (Figure 3a). Following equation (6), R^*_j was diagnosed for each initialized phytoplankton type at every time step and averaged over February. We show here the positive R^*_j for all the phytoplankton that coexist in this grid cell. (A negative R^*_j can denote a phytoplankton type for whom current local losses are larger than the growth. A negative R^*_j can also indicates phytoplankton types for whom local losses are balanced by the neglected transport terms.) Phytoplankton abundance increases with decreasing, positive R^*_j. Furthermore, the local concentration of the single limiting nutrient (dashed line in Figure 3a) closely matches $R^*_{\min}$, the lowest positive R^*_j of all the phytoplankton. Notably, in the illustrated global model, a single, lowest-R^* organism does not exclude all others, at least on the timescale of these integrations. Instead, several K strategist species with R^*_j close to $R^*_{\min}$ coexist (A. Barton et al., Modeling species diversity gradients in marine phytoplankton, manuscript in preparation, 2009). Those with similar R^*_j and high abundances have similar light and temperature requirements. Small variations in these environmental factors offer an opportunity for each species to be fittest at some point during the year, allowing coexistence on the longer term.

[22] On the other hand, the phytoplankton with higher R^*_j, but low abundances, are also K strategists which are not near their optimum temperature or light requirement (this will lead to a low ν_j and therefore high R^*_j). They may persist at low abundances due to lateral transport (immigration) or the timescale for their complete exclusion may be very long relative to the integration.

[23] Along a north-south transect in the Pacific (also for February) the ambient nutrient is almost identical to the R^*_j of the dominant species from −40° to the equator during the Southern Hemisphere summer (Figure 3b). However the nutrient is slightly higher than the R^*_j of the dominant species in the Northern Hemisphere reflecting a breakdown of the equilibrium balance assumed in equation (3) in the winter months (due to higher supply of nutrients and low growth rates during this period). Poleward of about 40° the nutrient concentration shows little or no correspondence to the $R^*_{\min}$, as anticipated since these regions are dominated instead by the r strategists.

[24] The tight coupling of growth and mortality in the tropics and subtropics, consistent with equation (3), breaks

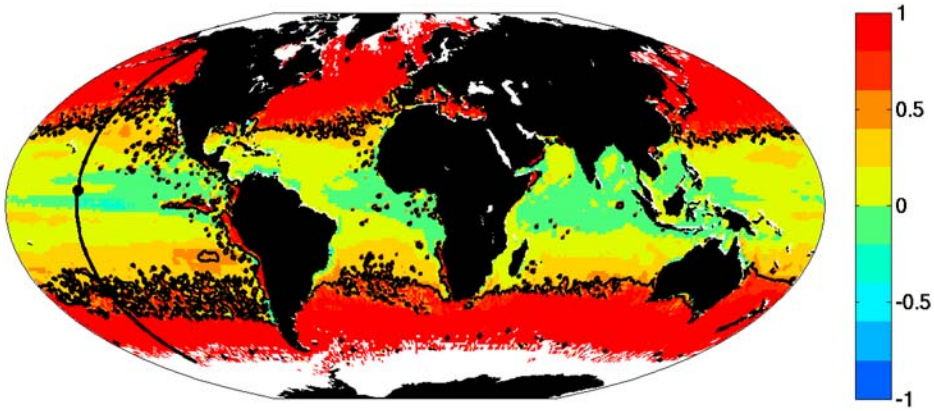

Figure 5. Single resource case: Ratio of difference to actual nutrient concentration $(N_1 - R^*_{\min})/(N_1)$. Contours are at (−0.5, 0.5), green/yellow shading indicate $R^*_{\min}$ close to ambient nutrient, red indicates nutrients exceed $R^*_{\min}$, and blue indicates that nutrients are less than the $R^*_{\min}$. No shading indicates where no reasonable value for the diagnosed $R^*_{\min}$ was found. Transect line and circle indicate locations for Figures 3 and 4.

down in the highly seasonal, subpolar oceans but may still be achieved during the summer period of the seasonal succession. $R^*_{\min}$ is similar to the ambient nutrient always in a tropical location (Figure 4b) but only during the summer in a higher-latitude location (Figure 4a). This is further revealed by the Hovmoller diagram (Figure 4c) of the variable $(N_1 - R^*_{\min})/N_1$, which measures the departure of the ambient concentration of the limiting resource from the minimum R^* of the organisms present, along the Pacific transect (Figure 4c). When $(N_1 - R^*_{\min})/N_1$ is close to zero (green/yellow) the equilibrium assumed in equation (3) is valid. In the tropical and subtropical waters, the equilibrium holds year round, between about 25° and 40° of latitude the balance holds seasonally in the summer. Poleward of 50°N in the Northern Hemisphere (sooner in the Southern Hemisphere), seasonal variations, advection and light limitation break the simple balance and drive nutrient concentrations away from $R^*_{\min}$.

[25] We also investigate (not shown here) the applicability of resource control theory with depth, and find that diagnosed $R^*_{\min}$ is close to the ambient nutrients for the lower latitudes from the surface down to about 50 m. At greater depths, low light leads to low growth rates and nutrient supply is higher, making the steady-state assumption less reasonable, and the $R^*_{\min}$ is a less useful diagnostic. For the remainder of the paper we will consider only the annual 0–50 m averaged results to examine the large-scale picture, but keep in mind that there are interesting time and depth-varying issues.

[26] In a global, annually averaged, perspective, the minimum positive, R^*_j ($R^*_{\min}$) of the phytoplankton types present closely anticipates the ambient concentration of the single nutrient in the tropics and subtropics. The interesting diagnostic to look at is, relatively, how much the ambient concentration of the limiting resource departs from $R^*_{\min}$: $(N_1 - R^*_{\min})/N_1$ (Figure 5). And consistent with the inference from the single Pacific transect the difference is small in the tropics and subtropics, but the equilibrium assumption breaks down in the extratropics. The region where the theory appears to hold is a subset of the domain where K strategy types dominate. Unshaded regions are those in which the pattern of $R^*_{\min}$ is particularly noisy or consistently negative. In such regions advection, decoupling of growth and grazing, or light limitation break the simple equilibrium assumed in equation (3).

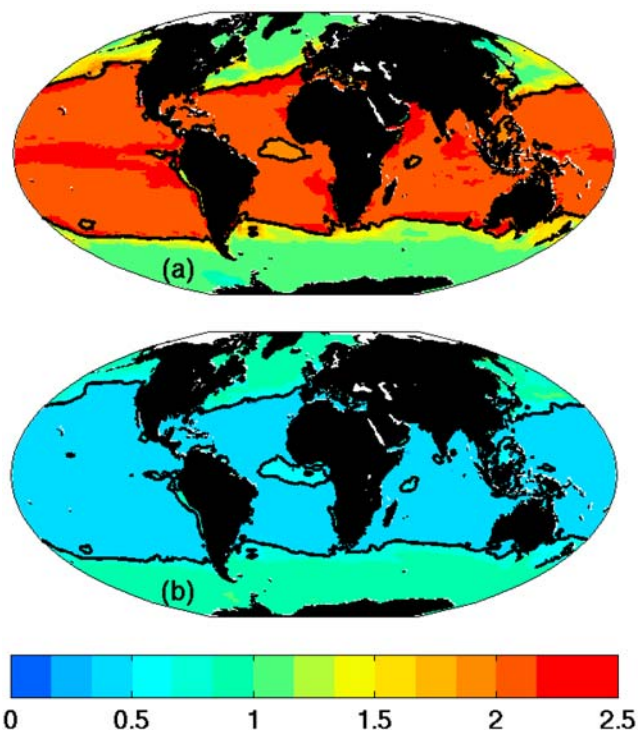

Figure 6. Single resource case, sensitivity experiments: Ratio of macronutrient in (a) double κ_{N_1} case; (b) halved κ_{N_1} case to macronutrient in control run (Figure 5). Contours are drawn at 2 (indicating nutrient concentrations double the control experiment) and at 0.5 (indicating nutrient concentrations half of the control experiment).

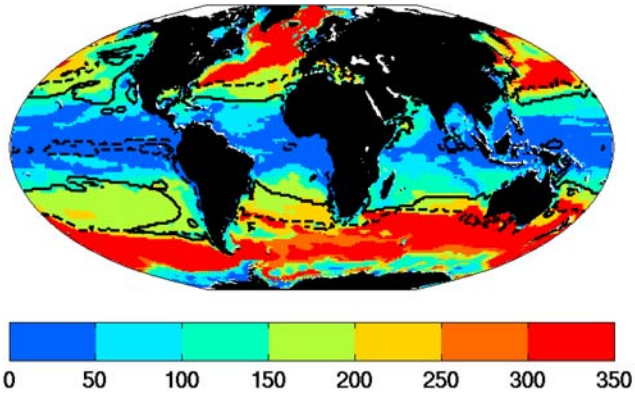

Figure 7. Relative stability of region: annual range of mixed layer depth (m). Mixed-layer depths are from ECCO-GODAE state estimates. [*Wunsch and Heimbach*, 2007]. Dashed contour indicates the region where the sensitivity studies in the single resource case show the expected linear relationship (0.5 and 2 contours from Figure 6). Solid line indicates where the *Prochlorococcus* analogs dominate in the multiple resource case (see Figure 11a).

2.3. Single Resource Case: Sensitivity Studies

[27] The power of resource competition theory to qualitatively and quantitatively interpret the low-seasonality region is most clearly demonstrated with additional sensitivity studies using the single resource configuration. The simple relationships equations (3) and (4) suggest a linear dependence of $\overline{N}$ on κ_{N_1}, while phytoplankton biomass $\overline{P}$ should be independent of this characteristic, providing that growth and mortality rates (μ_m and m) are relatively unaffected:

$$\frac{\partial \overline{N}}{\partial \kappa_{N_1}} = \frac{\partial R^*}{\partial \kappa_{N_1}} = \frac{m}{\mu_m - m} \tag{9}$$

$$\frac{\partial \overline{P}}{\partial \kappa_{N_1}} = 0 \tag{10}$$

Doubling and halving κ_{N_1} for all of the 78 initialized phytoplankton types, while all other parameters are held fixed, indeed reveals a linear response in minimum R^* and the ambient nutrient concentration over most of the low-seasonality regime where K strategy types dominate (Figures 6a and 6b). Consistently, total phytoplankton biomass is effectively unchanged (not shown). The predicted sensitivities are also seen in response to manipulations of growth and grazing rate (not shown).

[28] Thus, over a large areas of this idealized global ocean model the phytoplankton types that dominate the biomass, the ambient resource concentration, and the sensitivity of the resource concentration to changes in phytoplankton physiology, are all consistent with the expectations from the simple statement of resource competition theory encapsulated in equation (3). As expected, this framework has its greatest diagnostic ability in relatively stable physical environments where the simple assumption of equilibrium between growth and mortality is an appropriate balance. Here the ecological regime where the diagnostic R^* accurately describes the system is defined by a critical threshold in the annual range of mixed-layer depth (maximum mixed layer depth minus minimum) of about 250 m (Figure 7). This also reflects the transition between the extremely oligotrophic subtropical region and areas with higher surface nutrient concentration.

3. Multiple Resource Case

[29] Is this diagnostic framework useful in a more complex system? The single resource configuration is very idealized, with just two effective functional groups of phytoplankton, engineered to follow strictly r or K strategies. Variations in the light sensitivity of growth was removed, as well as the interaction with multiple, potentially limiting resources. We return now to a more realistic simulation [*Follows et al.*, 2007] which represents multiple limiting nutrients (several nitrogen species, phosphorus, iron and silica), variations in light sensitivity and palatability, as well as a generally more continuous range of physiologies (see section 1.2, *Follows et al.* [2007], Appendix A, and Tables 2 and 3 for details of the model). The initialized organisms in this case fall into four broad functional groups (Table 1), each consisting of multiple organisms: large fast growing eukaryotes with high-nutrient half-saturation constants, some of which use silica (diatom-analogs), small slower growing phytoplankton with high-nutrient affinity some of which cannot utilize nitrate (*Prochlorococcus* analogs). For these latter we assume an energetic trade-off leading to a lower half-saturation for dissolved nutrients. There are two explicit grazer populations with size-based prey palatability. How does resource competition theory help us interpret this more complex and realistic context?

Table 3. Ecosystem Model Parameters That Are Fixed for All Simulations

Parameter	Symbol	Fixed Value	Units
Temperature coefficients	A	1.04	
	C	4	
Temperature normalization	τ_1	0.33	
	τ_2	0.3	
Phytoplankton mortality	m^P	0.1	d^{-1}
Ammonium inhibition	ψ	4.6	$(\mu M\ N)^{-1}$
Maximum grazing rate	g_{max_a}	0.2	d^{-1}
	g_{max_b}	0.033	d^{-1}
Grazing half-saturation	κ^P	0.1	μM P
Zooplankton mortality	m^Z	0.033	d^{-1}
DOM remineralization rate	r_{DOP}	0.01	d^{-1}
	r_{DON}	0.01	d^{-1}
	r_{DOFe}	0.01	d^{-1}
DOM remineralization rate	r_{POP}	0.02	d^{-1}
	r_{PON}	0.02	d^{-1}
	r_{POFe}	0.02	d^{-1}
	r_{POSi}	0.0033	d^{-1}
POM sinking rate	w_{POM}	10	$m\ d^{-1}$
NH_4 to NO_2 oxidation rate	ζ_{NO2}	2	d^{-1}
NO_2 to NO_3 oxidation rate	ζ_{NH4}	0.1	d^{-1}
critical PAR for oxidation	I_{ox}	10	$\mu Ein\ m^{-2}\ s^{-1}$
Fe solubility constant	α_{Fe}	0.04	
Fe scavenging rate	c_{scav}	$1.1 * 10^{-3}$	d^{-1}
Ligand binding strength	β_{Fe}	$2 * 10^5$	$(\mu M)^{-1}$
PAR attenuation coefficient	k_o	0.04	m^{-1}
PAR attenuation from phytoplankton	k_P	0.64	$(\mu M\ P)^{-1}\ m^{-1}$

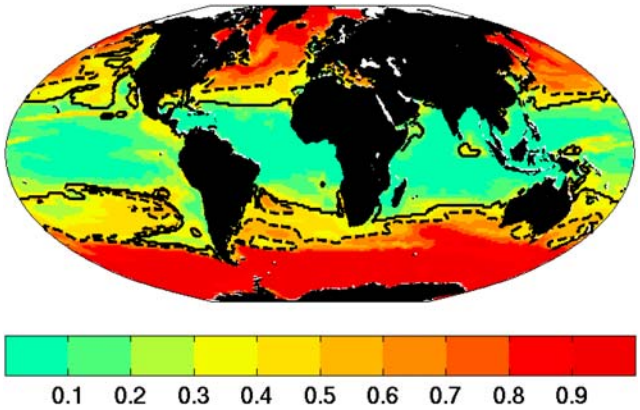

Figure 8. Multiple resource case: Average fraction of "r strategy" phytoplankton types (diatom and other large) relative to total biomass in the ensemble of runs. Dashed contour indicates 0.5; solid contour indicates range where *Prochlorococcus* analogs dominate (see Figure 11a).

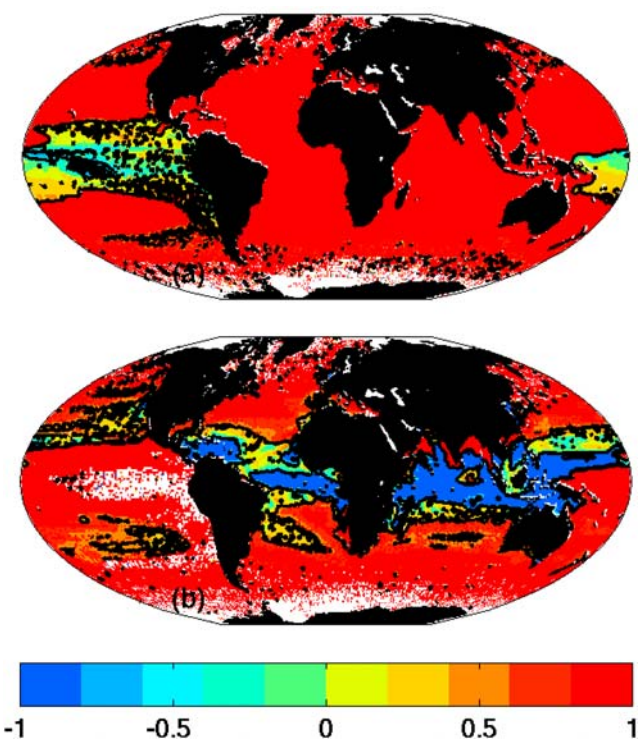

Figure 9. Multiple resource case: ratio of difference between minimum $R^*_{N_i}$ and the ambient nutrient concentration (a) $(Fe - R^*_{Fe_{\min}})/Fe$ and (b) $(NOx - R^*_{NOx_{\min}})/NOx$ where $NOx = NO3 + NO2$. Contours are at $(-0.5, 0.5)$, green/yellow shading indicates $R^*_{\min}$ close to ambient nutrient, red indicates nutrients exceed $R^*_{\min}$, and blue indicates that nutrients are less than the $R^*_{\min}$; no shading indicates where no reasonable value for the diagnosed $R^*_{\min}$ was found.

[30] An ensemble of 10 simulations was made, each with different randomization of physiological properties, and each integrated for 10 simulated years from identical initial conditions. The broad characteristics of community structure and productivity are plausible and robust between ensemble members. For the analysis of the multiple resource configuration we present averaged results from the 10 ensemble members.

[31] The biomass at high latitudes is strongly dominated by the fast growing phytoplankton including diatom analogs (Figure 8) while midlatitudes and low latitudes are dominated by the low-R^* phytoplankton, including the *Prochlorococcus* analogs which have the lowest R^*. This result echos the dominance by r and K strategy types in the illustrative, single resource model (Figure 2). However, in contrast to that configuration, the transition between ecological regimes is much gentler, with a more balanced mixture of functional types throughout the midlatitudes. This is enabled by the more continuous distribution of light sensitivities, palatabilities, nutrient half-saturation and multiple potentially limiting nutrients allowed in the "more realistic" configuration.

3.1. Multiple Resource Case: R^* Analysis

[32] In the multiple resource model we focus on an annual mean analysis. We examine the diagnostic R^* with reference to each potentially limiting nutrient. Here equation (A2) again assumes an equilibrium balance between growth and loss terms, neglecting transport. $R^*_{N_i,j}$ is calculated for each combination of nutrient and phytoplankton type. Iron

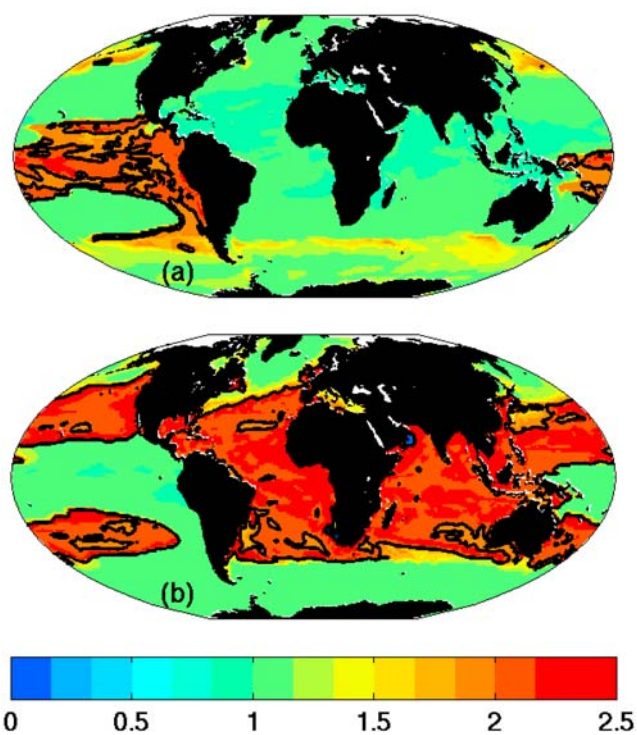

Figure 10. Multiple resource case, double κ_{N_i} sensitivity experiment: Ratio of (a) Fe and (b) NOx to that in the control run. Contours are drawn at 2 (indicating nutrient concentrations double the control experiment).

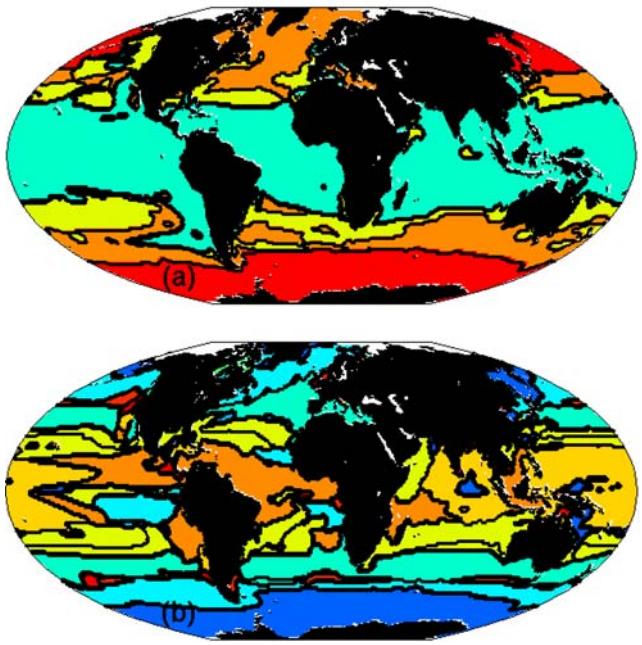

Figure 11. Multiple resource case: Annual mean emergent biogeographical provinces. (a) Biogeography of four major functional groups (from ensemble); mapping four regimes according to the relative contributions of four major "functional groups." The functional groups are determined by summing biomass contributions from four broad classes of initialized phytoplankton types: (1) diatom analogs (red), (2) other large phytoplankton (orange), (3) other small phytoplankton (yellow-green), and (4) *Prochlorococcus* analogs (dark green) [see *Follows et al.*, 2007]. (b) Ecotones from single ensemble member; lines where the ecosystem transitions from dominance by one phytoplankton type to another.

and nitrogen are the limiting resources in most areas of the model's oligotrophic subtropics and tropics and we focus our discussion on these elements. There are several forms of inorganic nitrogen resolved in the model, adding further complexity to the interpretation. Following the approach to the illustrative, single resource case, we compare the ambient surface iron concentration with the minimum $R^*_{Fe_{\min}}$, and the ambient oxidized forms of inorganic nitrogen, $NOx = NO_3 + NO_2$, with $R^*_{NOx_{\min}}$. Here we define:

$$R^*_{Fe_j} = \frac{\kappa_{Fe_j} L_j}{\nu_j - L_j}, \tag{11}$$

$$R^*_{NOx_j} = \frac{\kappa_{NOx_j}\left(L_j - \nu_j \dfrac{NH_4}{NH_4 + \kappa_{NH4_j}}\right)}{\nu_j\left(e^{-\psi NH_4} + \dfrac{NH_4}{NH_4 + \kappa_{NH4_j}}\right) - L_j}, \tag{12}$$

where ν_j and L_j are growth and loss terms defined in Appendix A (equations (A24) and (A25)). R^*_{NOx} includes additional terms reflecting the inhibition of nitrate and nitrite uptake when ammonium is plentiful. Again the R^* diagnostics reveal where resource competition theory provides an interpretation of the system in the oligotrophic, low-seasonality regimes, but also reflect the regional variations in limiting nutrient. In the low-latitude Pacific, where iron is the limiting nutrient, it is drawn down to a concentration close to that diagnosed from the physiology of the dominant organisms (Figure 9a) leaving a surfeit of inorganic nitrogen (Figure 9b) and phosphate. In much of the rest of the tropics/subtropics inorganic nitrogen is drawn down to close to or lower than the diagnosed values (Figure 9b), while iron (and phosphate) are in surfeit. The regions where nitrate is lower than expected are also those regions where model analogs of *Prochlorococcus* dominate. These organism are not able to utilize nitrate, and it is precisely these regions where there is insufficient nitrate where they are fittest and dominate the biomass (discussed further in section 3.3 and in the work of J. Bragg et al. (Modeling selective pressures on picocyanobacterial nitrogen use in the global ocean, submitted to *PLoS Biology*, 2009)).

3.2. Multiple Resource Case: Sensitivity Studies

[33] Sensitivity experiments, similar to those of section 2.3, more clearly elucidate and illustrate the relationship between ecosystem and nutrient concentrations in this multiple nutrient, multiple phytoplankton functional type case. Altering the half-saturation constants globally reveals the expected linear response in the ambient concentration of the locally limiting nutrient. In a sensitivity experiment where κ_{N_i} is doubled, we find that iron concentrations double in regions where iron is limiting (Figure 10a), but that there is no significant response from other nutrients in that region (Figure 10b). Similarly, in regions where nitrogen is limiting, we find a doubling of the *NOx* concentrations, but little change in the iron concentrations (Figures 10a and 10b).

[34] As in the illustrative single resource simulation, resource competition theory provides a powerful diagnostic framework for qualitative and quantitative analysis of the biogeochemical system. As in the illustrative case, this is true only in the more stable physical environments of the model, and only reflects the locally limiting resource; here one of several possible. The interaction of multiple forms of inorganic nitrogen complicates the interpretation of the analysis (a point anticipated by *Tilman* [1982]). The prediction of a linear relationship between half-saturation and ambient limiting nutrient is the most robust indication of where the simple equilibrium of equation (3) is relevant in this framework.

3.3. Multiple Resource Case: Biogeography

[35] In this more freely parameterized model, the basic organization of subtropical and tropical ecosystems echos that found in the single resource case. Within the region where the annual range of mixed-layer depth is less than 250 m the concentration of the limiting nutrient closely mirrors the lowest positive R^* of the initialized phytoplankton types, relative to that resource, of the phytoplankton present. Within this physical environment, changes to the phytoplankton physiology regulates the limiting nutrient in a predictable manner.

[36] Within the low-seasonality region, which favors K strategy types and is consistent with resource competition theory, there exists a further division delimiting the domain dominated by *Prochlorococcus* analogs (Figure 11a). In this model, *Prochlorococcus* analogs have been given an addi-

tional trade off: a lower-nutrient half-saturation constant for growth at the expense of the inability to utilize nitrate. Because of this, in the model *Prochlorococcus* analogs have the lowest R^* of any of the modeled phytoplankton. They dominate the region where mixed layer depth range is less than 100 m (solid contour in Figure 7). This is also the region where the annual range in temperature and incident photosynthetically available radiation (PAR) vary substantially less than other regions of the oceans. The very stable environment, and additional niche space enabled by the nitrate-use trade-off, leads to a subdivision of the oligotrophic region.

4. Discussion and Summary

[37] This study is at the interface of global biogeochemical cycles and marine ecology. We have examined the use of established ecological concepts as diagnostic tools for marine ecosystem and biogeochemistry models. We find that R^* is an appropriate measure of competitive ability in regions of low seasonality in a relatively complex model ocean ecosystem. In these most stable physical environments, it anticipates not only the outcomes of competition among phytoplankton, but quantitatively indicates the ambient concentration of the limiting nutrient and, most robustly, its sensitivity to changes in the physiological properties of organisms. Instead of finding a single, lowest-R^* organism excluding others, we found that several organisms with similarly low R^* could coexist. This feature is the subject of a detailed discussion elsewhere (A. Barton et al., manuscript in preparation, 2009).

[38] It is important to note that here, resource competition theory provides a useful diagnostic framework, and we have used it as such. It provides a means with which to elucidate and illustrate the intimate connection between the resource environment and the organisms which inhabit it. Because the mortality of the phytoplankton in our global model is a complex function of their abundance, and that of their predators, a simple prognosis of the lowest R^* and ambient nutrient concentration possible with highly idealized forms is not possible. This does not, however, devalue the powerful insight provided by this framework.

[39] An illustrative single resource model was initialized with 39 phytoplankton pairs, each consisting of an r strategy type and a K strategy type. This model displayed two broad ecological regimes; separated by physical environment, seasonal and stable, and dominated by r and K strategy functional types, respectively. The boundary between the two regimes occurs where the seasonal range of mixed-layer depth reaches about 250 m in this model (Figure 7) and at the boundary between low-nutrient and high-nutrient regimes. In contrast, the physiologically and ecologically richer "multiple resource case" exhibits a more complex biogeography. The two, broad biogeographical regimes of the single-resource case fragment into finer-scale patterns. Defining and mapping four broad functional groups (Figure 11a; *Prochlorococcus* analogs, other small phytoplankton, diatom analogs, other large eukaryotes) reveals additional meridional structure, also coincident with isolines of mixed-layer seasonal range. The 100 m isoline (Figure 7) demarcates the domain dominated by *Prochlorococcus* analogs, which in this case have the lowest R^*s of all. The strong physical control of the ecological and biogeographic provinces has long been recognized [e.g., *Longhurst*, 1998].

[40] It is interesting to step back from the categorization of functional groups in the richer, multiple resource solution. Figure 11b illustrates the general biogeography of the model solution depicted by marking the ecological boundaries where the ecosystem transitions from dominance by one phytoplankton type to another. Remarkably, and pleasingly, the model ecosystem's emergent biogeography closely reflects that revealed by more classical analyzes of marine provinces [*Longhurst*, 1998] as well as recent analyzes based largely on remote observations [*Oliver and Irwin*, 2008]. This model's emergent biogeography exhibits a similar number of provinces, with closely matching geographical patterns.

[41] That the emergent ecological provinces closely match those observed suggests that the ecosystem model captures appropriately some of the fundamental organizing processes which are at work in the oceans. That we can use established ecological concepts to qualitatively and quantitatively interpret at least the coarse-grained distribution of functional groups and their control on nutrient distributions is very encouraging. We anticipate refining the R^* diagnostic used here in future studies to help us elucidate further the links between the physical environment and the ecological regimes denoted by these provinces.

[42] In summary, this study emphasizes the close ties between marine biogeochemical cycles, ecological regimes and the physical environment. We have used a self-assembling global marine ecosystem and biogeochemistry model to explore the organization of phytoplankton communities and their role in regulating limiting nutrients. We have demonstrated the resource competition theory provides a useful framework for interpreting these ecological-biogeochemical interactions in the more stable physical regions of the subtropical and tropical oceans. Our study therefore supports the emphasis of recent studies [*Falkowski and Oliver*, 2007; *Wilson et al.*, 2007; *Litchman et al.*, 2007; *Tozzi et al.*, 2004] on R^*. The seasonality of the surface ocean environment is a key organizing factor for marine ecosystems and can be used to demarcate the boundaries of coarse grained provinces dominated by particular functional groups in the model. Pleasingly, the model's emergent biogeography maps closely into that interpreted by classical approaches. Resource competition theory provides a robust interpretive framework for some regions in the complex model, at least for appropriate biogeographical regimes.

Appendix A: Ecosystem Model Parameterization

[43] The ecosystem model equations are similar to that used by *Follows et al.* [2007]. We direct the reader to the online supplemental material of that paper for additional discussion. The most significant change is that the grazing term is now includes variable palatability of phytoplankton and sloppy feeding as treated by *Dutkiewicz et al.* [2005]. Additionally the nitrogen limitation term (equation (A10)) has been slightly modified.

[44] Several nutrients N_i nourish many phytoplankton types P_j which are grazed by several zooplankton types Z_k. Mortality of and excretion from plankton, and sloppy feeding by zooplankton contribute to a dissolved organic matter DOM_i pool and a sinking particulate organic matter pool POM_i. Subscript i refers to a nutrient/element, j for a specific phytoplankton type, and k for a zooplankton type.

$$\frac{\partial N_i}{\partial t} = -\nabla\cdot(\mathbf{u}N_i) + \nabla\cdot(K\nabla N_i) - \sum_j \left[\mu_j P_j M_{ij}\right] + S_{N_i} \tag{A1}$$

$$\frac{\partial P_j}{\partial t} = -\nabla\cdot(\mathbf{u}P_j) + \nabla\cdot(K\nabla P_j) + \mu_j P_j - m_j^P P_j - \sum_k \left[g_{jk} Z_{k,i=1}\right] - \frac{\partial(w_j^P P_j)}{\partial z} \tag{A2}$$

$$\frac{\partial Z_{ki}}{\partial t} = -\nabla\cdot(\mathbf{u}Z_{ki}) + \nabla\cdot(K\nabla Z_{ki}) + Z_{ki}\sum_j \left[\zeta_{jk} g_{jk} M_{ij}\right] - m_k^Z Z_{ki} \tag{A3}$$

$$\frac{\partial POM_i}{\partial t} = -\nabla\cdot(\mathbf{u}POM_i) + \nabla\cdot(K\nabla POM_i) - r_{POM_i} POM_i - \frac{\partial(w_{POM_i} POM_i)}{\partial z} + S_{POM_i} \tag{A4}$$

$$\frac{\partial DOM_i}{\partial t} = -\nabla\cdot(\mathbf{u}DOM_i) + \nabla\cdot(K\nabla DOM_i) - r_{DOM_i} DOM_i + S_{DOM_i} \tag{A5}$$

where

- $\mathbf{u}$ velocity in physical model, = (u, v, w);
- K Mixing coefficients used in physical model;
- z Depth;
- μ_j Growth rate of phytoplankton j (see below);
- M_{ij} Matrix of Redfield ratio of element i to phosphorus for phytoplankton j;
- ζ_{jk} Grazing efficiency of zooplankton k on phytoplankton j (represents sloppy feeding);
- g_{jk} Grazing of zooplankton k on phytoplankton j (see below);
- m_j^P Mortality/Excretion rate for phytoplankton j;
- m_k^Z Mortality/Excretion rate for zooplankton k;
- w_j^P Sinking rate for phytoplankton j;
- w_{POM_i} Sinking rate for POM i;
- r_{DOM_i} Remineralization rate of DOM for element i;
- r_{POM_i} Remineralization rate of POM for element i;
- S_{N_i} Additional source or sink for nutrient i (see below);
- S_{DOM_i} Source of DOM of element i (see below);
- S_{POM_i} Source of POM of element i (see below).

A1. Phytoplankton Growth

[45]

$$\mu_j = \mu_{\max_j} \gamma_j^T \gamma_j^I \gamma_j^N \tag{A6}$$

where

- $\mu_{\max_j}$ Maximum growth rate of phytoplankton j;
- γ_j^T Modification of growth rate by temperature for phytoplankton j;
- γ_j^I Modification of growth rate by light for phytoplankton j;
- γ_j^N Modification of growth rate by nutrients for phytoplankton j.

[46] Temperature modification (Figure 1a):

$$\gamma_j^T = \frac{1}{\tau_1}\left(A^T e^{-B(T-T_o)^c} - \tau_2\right) \tag{A7}$$

where coefficients τ_1 and τ_2 normalize the maximum value, and A,B,T_o and C regulate the form of the temperature modification function. T is the local model ocean temperature.

[47] Light modification (Figure 1b):

$$\gamma_j^I = \frac{1}{F_o}\left(1 - e^{-k_{par} I}\right) e^{-k_{inhib} I} \tag{A8}$$

where F_o is a factor controlling the maximum value, k_{par} is the PAR saturation coefficient and k_{inhib} is the PAR inhibition factor. I is the local PAR, that has been attenuated through the water column (including the effects of self-shading).

[48] Nutrient limitation is determined by the most limiting nutrient:

$$\gamma_j^N = \min(N_i^{lim}) \tag{A9}$$

where typically $N_i^{lim} = \frac{N_i}{N_i + \kappa_{N_{ij}}}$ (Figure 1c) and $\kappa_{N_{ij}}$ is the half-saturation constant of nutrient i for phytoplankton j.

[49] When we include the nitrogen as a potential limiting nutrient we modify N_i^{lim} to take into account the uptake inhibition caused by ammonium:

$$N_N^{lim} = \frac{NO_3 + NO_2}{NO_3 + NO_2 + \kappa_{NOx_j}} e^{\psi NH_4} + \frac{NH_4}{NH_4 + \kappa_{NH4_j}} \tag{A10}$$

where ψ reflects the inhibition and κ_{NOx_j} and κ_{NH4_j} are the half-saturation constant of $NOx = NO_3 + NO_2$ and NH_4, respectively.

A2. Zooplankton Grazing

[50]

$$g_{jk} = g_{\max_{jk}} \frac{\eta_{jk} P_j}{A_k} \frac{A_k}{A_k + \kappa_k^P} \tag{A11}$$

where

- $g_{\max_{jk}}$ Maximum grazing rate of zooplankton k on phytoplankton j;
- η_{jk} Palatability of plankton j to zooplankton k;
- A_k Palatability (for zooplankton k) weighted total phytoplankton concentration, = $\Sigma_j \eta_{jk} P_j$;
- κ_k^P Half-saturation constant for grazing of zooplankton k;

The maximum grazing $g_{\max_{jk}}$ depends of the relative size of the phytoplankton j and zooplankton k, with a faster rate if

they are both small or both big ($g_{\max_a}$), and slower if they are in different size classes ($g_{\max_b}$).

A3. Inorganic Nutrient Source/Sink Terms

[51] S_{N_i} depends on the specific nutrient, and includes the remineralization of organic matter, external sources and other nonbiological transformations:

$$S_{PO4} = r_{DOP}DOP + r_{POP}POP \tag{A12}$$

$$S_{Si} = r_{POSi}POSi \tag{A13}$$

$$S_{FeT} = r_{DOFe}DOFe + r_{POFe}POFe - c_{scav}Fe' + \alpha F_{atmos} \tag{A14}$$

$$S_{NO3} = \zeta_{NO3}NO_2 \tag{A15}$$

$$S_{NO2} = \zeta_{NO2}NH4 - \zeta_{NO3}NO_2 \tag{A16}$$

$$S_{NH4} = r_{DON}DON + r_{PON}PON \tag{A17}$$

where

- r_{DOM_i} Remineralization rate of DOM for element i, here P, Fe, N;
- r_{POM_i} Remineralization rate of POM for element i, here P, Si, Fe, N;
- c_{scav} scavenging rate for free iron;
- Fe' free iron, modeled as by *Parekh et al.* [2005];
- α solubility of iron dust in ocean water;
- F_{atmos} atmospheric deposition of iron dust on surface of model ocean;
- ζ_{NO3} oxidation rate of NO_2 to NO_3;
- ζ_{NO2} oxidation rate of NH_4 to NO_2 (is photoinhibited).

[52] The remineralization timescale r_{DOM_i} and r_{POM_i} parameterizes the break down of organic matter to an inorganic form through the microbial loop.

A4. DOM and POM Source Terms

[53] S_{DOM_i} and S_{POM_i} are the sources of dissolved and particulate organic detritus arising from mortality, excretion and sloppy feeding of the plankton. We simply define that a fixed fraction λ_m of the mortality/excretion term and the nonconsumed grazed phytoplankton (λ_g) go into the dissolved pool and the remainder into the particulate pool.

$$S_{DOM_i} = \sum_j \left[\lambda_{mp_{ij}} m_j^p P_j M_{ij}\right] + \sum_k \left[\lambda_{mz_{ik}} m_k^z Z_{ki}\right] + \sum_k \sum_j \left[\lambda_{g_{ijk}}(1-\zeta_{jk}) g_{ij} M_{ij} Z_{ki}\right] \tag{A18}$$

$$S_{POM_i} = \sum_j \left[(1-\lambda_{m_{pij}}) m_j^p P_j M_{ij}\right] + \sum_k \left[(1-\lambda_{mz_{ik}}) m_k^z Z_{ki}\right] + \sum_k \sum_j \left[(1-\lambda_{g_{ijk}})(1-\zeta_{jk}) g_{ij} M_{ij} Z_{ki}\right] \tag{A19}$$

A5. Assignment of Phytoplankton Physiological Functionality and Growth Rate Sensitivity

[54] In the multiple resource case (section 3), the physiological functionality and sensitivity of growth to temperature, light and ambient nutrient abundance for each modeled phytoplankton type is governed by several true/false parameters, the values of which are based on a virtual "coin toss" at the initialization of each phytoplankton type. Coin tosses determine the size class of each phytoplankton type ("large" or "small"), whether the organism can assimilate nitrate, whether the organism can assimilate nitrite, and whether the organism requires silicic acid. Parameter values which regulate the effect of temperature, light and nutrient availability on growth, are then assigned stochastically from within reasonable ranges specific for each size class. Some simple allometric trade-offs are imposed (Figure 1b): Phytoplankton in the large size class are distinguished by higher intrinsic maximum growth rates and faster sinking speeds [*Laws*, 1975]. They also draw parameter values from distributions with higher-nutrient half-saturations (assuming they are less efficient at acquiring nutrients [*Gavis*, 1976]) and are assumed to be high light adapted due to packaging effects [*Ravin and Falkowski*, 1997; *Finkel*, 2001].

[55] In the illustrative single resource case (section 2), the parameters are set specifically to obtain pairs of fast growing K strategist and slow growing r strategists, and only one zooplankton.

[56] For more discussion and the choices of parameters see the online supplemental material of *Follows et al.* [2007]. Tables 2 and 3 show the parameters used in the experiments discussed here.

A6. Derivation of Numerical Model R^* Diagnostic

[57] The equations for the numerical simulation (A1–A5) are far more complex than the simple system discussed in section 1.1, however we can still solve for a R^* diagnostic. We take equation (A2) assume steady state and neglect the transport terms (this latter assumption could be changed, and a future project will address this). Growth μ_j includes a function for the most limiting nutrient γ_j^N (equation (A9)) which for most nutrients, i, is a Monod function $\frac{N_i}{N_i+\kappa_{N_{ij}}}$. We can thus have an equation for each N_i (where N_i is phosphate, iron or silicic acid) and each phytoplankton P_j:

$$0 = \mu_{\max_j}\gamma_j^T\gamma_j^I \frac{N_i}{N_i+\kappa_{N_{ij}}} P_j - m_j^P P_j - \sum_k \left[g_{jk} Z_{k,i=1}\right] - \frac{\partial(w_j^P P_j)}{\partial z}$$

and for nitrate and nitrite where the Monod function has been modified for the preferential uptake of ammonium:

$$0 = \mu_{\max_j}\gamma_j^T\gamma_j^I \left(\frac{NO_3+NO_2}{NO_3+NO_2+\kappa_{NOx_j}} e^{\psi NH_4} + \frac{NH_4}{NH_4+\kappa_{NH4_j}}\right) P_j - m_j^P P_j - \sum_k \left[g_{jk} Z_{k,i=1}\right] - \frac{\partial(w_j^P P_j)}{\partial z}.$$

The above equations can be solved for the steady state nutrient concentrations, or $R^*_{N_j}$:

$$R^*_{PO4_j} = \frac{\kappa_{PO4_j} L_j}{\nu_j - L_j}, \tag{A20}$$

$$R^*_{Fe_j} = \frac{\kappa_{Fe_j} L_j}{\nu_j - L_j}, \tag{A21}$$

$$R^*_{Si_j} = \frac{\kappa_{Si_j} L_j}{\nu_j - L_j}, \tag{A22}$$

$$R^*_{NOx_j} = \frac{\kappa_{NOx_j}\left(L_j - \nu_j \dfrac{NH_4}{NH_4 + \kappa_{NH4_j}}\right)}{\nu_j\left(e^{-\psi NH_4} + \dfrac{NH_4}{NH_4 + \kappa_{NH4_j}}\right) - L_j}, \tag{A23}$$

where

$$\nu_j = \mu_{\max_j} \gamma_j^T \gamma_j^I \tag{A24}$$

$$L_j = m_j^p + \frac{1}{P_j}\frac{\partial w_j^p P_j}{\partial z} + \sum_k g_{\max_{jk}} \frac{\eta_{jk}}{A_k} \frac{A_k}{A_k + \kappa_k^P} Z_{k,i=1}. \tag{A25}$$

Here the growth term, ν_j, is a function of temperature and light and the loss term, L_j, includes mortality, sinking and grazing by multiple grazers. This loss term is a function of the abundance of the jth phytoplankton, the total palatability weighted abundance of phytoplankton concentration A_k, and the abundance of grazer Z_k. In essence R^* is still a combination of the phytoplankton physiology and the loss terms, however the nonlinearity means that R^* is no longer independent of the phytoplankton and source terms.

[58] **Acknowledgments.** The ocean circulation state estimates used in this study were kindly provided by the Estimating the Circulation and Climate of the Ocean (ECCO) Consortium funded by the National Oceanographic Partnership Program (NOPP). We thank Patrick Heimbach in particular for his assistance. We appreciate many interesting discussions with Fanny Monteiro and Andrew Barton. Comments from Kelly Kryc and two anonymous reviewers substantially improved this paper. M.J.F. is grateful to Paul Falkowski for first introducing him to resource competition theory. We are grateful for support from the Gordon and Betty Moore Foundation and the National Science Foundation.

References

Armstrong, R., C. Lee, J. Hedges, S. Honjo, and S. Wakeham (2002), A new, mechanistic model for organic carbon fluxes in the ocean: Based on the quantitative association of POC with ballast minerals, *Deep Sea Res., II*, *49*, 219–236.

Armstrong, R. A., and R. McGehee (1980), Competitive exclusion, *Am. Nat.*, *115*, 151–170.

Conkright, M. E., H. E. Garcia, T. D. O'Brien, R. A. Locarnini, T. P. Boyer, C. Stephens, and J. I. Antonov (2002), World Ocean Atlas 2001, vol. 4, Nutrients, in *NOAA Atlas NESDIS*52, U.S. Govt. Print. Off., Washington, D. C.

Dutkiewicz, S., M. Follows, and P. Parekh (2005), Interactions of the iron and phosphorus cycles: A three-dimensional model study, *Global Biogeochem. Cycles*, *19*, GB1021, doi:10.1029/2004GB002342.

Falkowski, P. G., and M. J. Oliver (2007), Mix and match: How climate selects phytoplankton, *Nat. Rev. Microbiol.*, *5*, 813–819.

Finkel, Z. V. (2001), Light absorption and the size scaling of light-limited growth and photosynthesis in marine diatoms, *Limnol. Oceanogr.*, *46*, 86–94.

Follows, M. J., S. Dutkiewicz, S. Grant, and S. W. Chisholm (2007), Emergent biogeography of microbial communities in a model ocean, *Science*, *315*, 1843–1846.

Gavis, J. (1976), Munk and Riley revisited: Nutrient diffusion, transport and rates of phytoplankton growth, *J. Mar. Res.*, *34*, 161–179.

Hood, R. R., et al. (2006), Pelagic functional group modeling: Progress, challenges and prospects, *Deep Sea Res., II*, *53*, 459–512.

Irwin, A. J., Z. V. Finkel, O. Schofield, and P. G. Falkowski (2006), Scaling-up from nutrient physiology to the size structure of phytoplankton communities, *J. Plankton Res*, *28*, 459–471.

Kilham, P., and R. E. Hecky (1988), Comparative ecology of marine and freshwater phytoplankton, *Limnol. Oceanogr.*, *33*, 776–795.

Klaas, C., and D. Archer (2002), Association of sinking organic matter with various types of mineral ballast in the deep sea: Implications for the rain ratio, *Global Biogeochem. Cycles*, *16*(4), 1116, doi:10.1029/2001GB001765.

Laws, E. A. (1975), The importance of respiration losses in controlling the size distribution of marine phytoplankton, *Ecology*, *56*, 419–426.

Laws, E. A., P. G. Falkowski, W. O. Smith, H. Ducklow, and J. J. McCarthy (2000), Temperature effects on export production in the open ocean, *Global Biogeochem. Cycles*, *14*, 1231–1246.

Le Quéré, C., et al. (2005), Ecosystem dynamics based on plankton functional types for global ocean biogeochemistry models, *Global Change Biol.*, *11*, 2016–2040.

Litchman, E., C. A. Klausmeier, O. M. Schofield, and P. G. Falkowski (2007), The role of functional traits and trade-offs in structuring phytoplankton communities: Scaling from cellular to ecosystem level, *Ecol. Let.*, *10*, 1170–1181.

Longhurst, A. (1998), *Ecological Geography of the Sea*, 398 pp., Acad. Press, San Diego, Calif.

Margalef, R. (1968), *Perspectives in Ecological Theory*, 111 pp., Univ. of Chicago Press, Chicago, Ill.

Marshall, J. C., C. Hill, L. Perelman, and A. Adcroft (1997), Hydrostatic, quasi-hydrostatic and non-hydrostatic ocean modeling, *J. Geophys. Res.*, *102*, 5733–5752.

McArthur, R. H., and E. O. Wilson (1967), *The Theory of Island Biogeography*, 203 pp., Princeton Univ. Press, Princeton, N. J.

Moore, J., S. Doney, D. Glover, and I. Fung (2002), Iron cycling and nutrient-limitation patterns in surface waters of the world ocean, *Deep Sea Res., II*, *49*, 463–507.

Oliver, M. J., and A. J. Irwin (2008), Objective global ocean biogeographic provinces, *Geophys. Res. Lett.*, *35*, L15601, doi:10.1029/2008GL034238.

Parekh, P., M. J. Follows, and E. A. Boyle (2005), Decoupling of iron and phosphate in the global ocean, *Global Biogeochem. Cycles*, *19*, doi:10.1029/2004GB002280.

Pomeroy, L. R. (1974), The ocean's food web, a changing paradigm, *Bioscience*, *24*, 499–504.

Ravin, J., and P. G. Falkowski (1997), *Aquatic Photosynthesis*, 375 pp., Blackwell Sci., Malden, Mass.

Stewart, F. M., and B. R. Levin (1973), Partitioning of resources and the outcome of interspecific competition: A model and some general considerations, *Am. Nat.*, *107*, 171–198.

Tilman, D. (1977), Resource competition between planktonic algae: An experimental and theoretical approach, *Ecology*, *58*, 338–348.

Tilman, D. (1982), *Resource Competition and Community Structure*, *Monogr. in Pop. Biol.*, vol. 17, 296 pp., Princeton Univ. Press, Princeton, N. J.

Tozzi, S., O. Schofield, and P. Falkowski (2004), Historical climate change and ocean turbulence as selective agents for two key phytoplanktonfunctional groups, *Mar. Ecol. Prog. Ser.*, *274*, 123–132.

Wilson, J. B., E. Spijkerman, and J. Huisman (2007), Is there really insufficient support for Tilman's R* Concept? A comment on Miller et al., *Am. Nat.*, *169*, 700–706.

Wunsch, C., and P. Heimbach (2007), Practical global ocean state estimation, *Physica D*, *230*, 197–208.

J. G. Bragg, CSIRO Plant Industry, Canberra, ACT 2601, Australia.

S. Dutkiewicz and M. J. Follows, Department of Earth, Atmospheric and Planetary Sciences, Massachusetts Institute of Technology, 54-1412, 77 Massachusetts Avenue, Cambridge, MA 02139, USA. (stephd@ocean.mit.edu)